Enhancing Curcumin Anticancer Efficacy Through Di-Block Copolymer Micelle Encapsulation

Article *in* Journal of Biomedical Nanotechnology · February 2014

DOI: 10.1166/jbn.2014.1809 · Source: PubMed

9 authors, including:

Li Lv
Shanghai Jiao Tong University
9 PUBLICATIONS **147** CITATIONS

SEE PROFILE

Yuanyuan Shen
China academy of fine arts
45 PUBLICATIONS **423** CITATIONS

SEE PROFILE

Jieying Liu
Peking Union Medical College Hospital
17 PUBLICATIONS **166** CITATIONS

SEE PROFILE

Feihu Wang
Shanghai Jiao Tong University
29 PUBLICATIONS **881** CITATIONS

SEE PROFILE

Article

Journal of Biomedical Nanotechnology
Vol. 10, 1–15, 2014
www.aspbs.com/jbn

Enhancing Curcumin Anticancer Efficacy Through Di-Block Copolymer Micelle Encapsulation

Li Lv[1], Yuanyuan Shen[1], Jieying Liu[1], Feihu Wang[1], Min Li[1], Mingna Li[1], Aijie Guo[1], Yun Wang[1], Dejian Zhou[2,*], and Shengrong Guo[1,*]

[1] *School of Pharmacy, Shanghai Jiao Tong University, Shanghai, 200240, China*
[2] *School of Chemistry and Astbury Centre for Structural Molecular Biology, University of Leeds, UK*

We report herein the development of a novel aqueous formulation and improved antitumor activity for curcumin by encapsulating it into a biocompatible and biodegradable poly(L-lactic acid) based poly(anhydride-ester)-*b*-poly(ethylene glycol) (PAE-*b*-PEG) micelle. The resulting curcumin loaded micelles were completely water-dispersible, overcoming the problem of poor water solubility that limited its efficacy and bioavailability. *In vitro* cellular studies revealed that the curcumin-loaded micelles were taken up mainly via endocytosis route and exhibited higher cytotoxicities toward model cancer cell lines (HeLa and EMT6) than free curcumin. An *in vivo* biodistribution study revealed that the curcumin-loaded micelles displayed significantly enhanced accumulation inside the tumor of EMT6 breast tumor-bearing mice. More impressively, the curcumin-loaded micelles showed stronger antitumor activity, higher anti-angiogenesis effects and induced apoptosis on the EMT6 breast tumor model bearing mice than free curcumin. Furthermore, the curcumin-loaded micelles showed no significant toxicity towards hemotological system, major organs or tissues in mice. Combined with a high antitumor activity and low toxic side-effects, the curcumin-loaded micelles developed here thus appear to be a highly attractive nanomedicine for effective, targeted cancer therapy.

KEYWORDS: *Nanomedicine, Cancer Therapy, Curcumin, Block Copolymer Micelle, Biodistribution.*

INTRODUCTION

Curcumin (Cur), a natural diphenol containing compound extracted from the ground rhizomes of *curcuma longa*, possesses a number of highly beneficial biological and therapeutic properties, including anticancer and chemoprevention.[1–4] Previous studies have shown that Cur is a universal anticancer agent capable of suppressing many types of cancers, including cervical, breast, lung, colorectal, pancreatic and prostate carcinomas, by providing anti-angiogenesis function and inducing tumor cell apoptosis.[5–9] Despite these highly encouraging findings, its application in anticancer therapy *in vivo* has been severely limited by its intrinsic properties such as low aqueous solubility and poor stability, leading to poor bioavailability and extensive first pass metabolism.[10,11] Moreover, being a small-molecule drug, Cur enters cells mostly by passive diffusion, lacking of specific targeting ability that is key to reducing toxic side-effects. Therefore, it is important to develop a robust, novel aqueous nanoscale formulation that can offer targeted delivery and controlled intracellular release properties to further enhance its therapeutic efficacy and reduce undesirable side-effects.

Over the past twenty years, several nanotechnology based approaches have been developed to overcome the poor water-solubility of lipophilic drugs,[12–20] among which, drug encapsulation into nanoscale carriers, such as liposomes[17] and polymeric nanoparticles[18] or micelles[20] have been most often exploited. These approaches can render the hydrophobic drug completely dispersible in water, making the drug intravenously injectable. In this regard, polymeric micelles are highly attractive, such nanoscale assemblies of amphiphilic polymers where their hydrophobic domains are packed together to form a hydrophobic core that can serve as a potent nanocontainer for hydrophobic drugs, while the hydrophilic segments are exposed forming a hydrophilic shell to stabilize their dispersion in the aqueous environment.[8] Encapsulation of hydrophobic

*Authors to whom correspondence should be addressed.
Emails: d.zhou@leeds.ac.uk, srguo@sjtu.edu.cn
Received: 12 July 2013
Accepted: 4 September 2013

drugs into nanoscale polymeric micelles can enhance antitumor efficacy and reduce side effects for small-molecule drugs, owing to their nanoscale sizes, allowing them to achieve enhanced accumulation inside tumors via the enhanced permeability and retention (EPR) effect, a characteristic pathological property of solid tumours.[21]

For effective drug delivery, an ideal polymer drug carrier should process several properties: non-toxic, biocompatible and biodegradable, allowing efficient clearance from the body after drug delivery. In this regard, amphiphilic block copolymers have been used extensively in broad range of pharmaceutical and drug delivery applications, ranging from sustained-release technology to gene delivery.[22, 23] In an aqueous solution, they form stable micelles with a hydrophobic inner core that can be used for convenient and efficient encapsulation of hydrophobic drugs while the exposed hydrophilic outer shell allows them to form stable dispersion at above the critical micelle concentration (CMC). Previously, we have synthesized a novel, amphiphilic poly(anhydride-esters)-*b*-poly(ethylene glycol) copolymer (PAE-*b*-PEG) by esterification of methyl poly(ethylene glycol) and poly (anhydride-esters) via melting polycondensation of α-, ω-acetic anhydride terminated poly(L-lactic acid). The number-average molecular weight of the obtained PAE-*b*-PEG was 7260 Da and the polydispersity was 2.31. Its CMC was 3.78 μg/mL.[24]

Several polymeric micelles have been used as Cur nanocarriers, such as poloxamer,[20] poly(ethyleneglycol)-poly(ε-capro-lactone),[8, 9] poly(ethyleneglycol)-*b*-poly(ε-caprolactone-co-*p*-dioxanone) micelles.[3] These polymers are all polyester based, which usually undergo bulk erosion and degrade slowly (slow drug release),[25] whereas polyanhydrides generally undergo surface erosion and degrade rapidly (fast drug release). It is therefore difficult to achieve controlled release, an important factor for efficient drug delivery, by either polymer alone. On the other hand, poly(anhydride-esters) which combine both poly(anhydrides) and polyesters can achieve controlled drug release readily by tuning the relevant abundance of the two polymers, making them highly attractive in drug delivery applications.[26]

This study aims to develop a novel aqueous nanoformulation of Cur using a biocompatible and biodegradable poly(L-lactic acid) based poly(anhydride-ester)-*b*-poly(ethylene glycol) (PAE-*b*-PEG) micelle as the drug nanocarrier to take the advantageous, controlled release properties of poly(anhydride ester) and evaluate its anti-cancer efficacy at both cellular and *in vivo* mouse model levels. We found that Cur can be efficiently encapsulated into such polymer micelles, forming a stable nanoformulation that can offer controlled, sustained drug release with significantly enhanced cytotoxicity towards cancer cells over free Cur. Moreover, it also exhibited significantly enhanced accumulation inside the tumor, and offering more potent anticancer and anti-angiogenesis efficacies than free Cur toward tumor bearing mice. Furthermore, the Cur-micelles showed no observable *in vivo* toxicity and appear to be safe.

MATERIALS AND METHODS

Materials

Curcumin (purity, 98%) was purchased from Alfa-Aesar. Dulbecco's modified eagle's medium (DMEM) was purchased from Invitrogen Corporation (Grand Island, USA). Penicillin-streptomycin, fetal bovine serum (FBS), 0.25% (w/v) trypsine, 0.03% (w/v) Ethylene Diamine Tetraacetie Acid (EDTA) solution, phosphate-buffered saline (PBS), 3-(4,5-dimethylthiazol-2-yl)-2, 5-diphenyltetrazolium bromide (MTT) and dimethylsulfoxide (DMSO) were purchased from Solarbio Science and Technology (Beijing, China).

Preparation of Cur Loaded PAE-*b*-PEG Micelles

Cur loaded PAE-*b*-PEG micelles were prepared by using a solid dispersion method.[3] Briefly, 5 mg of Cur was mixed with 50 mg of PAE-*b*-PEG copolymers in 10 mL of dichloromethane, followed by sonication at room temperature for 30 min. Then, the solution was evaporated to dryness on a rotary evaporator under reduced pressure at 40 °C for 1 h to obtain a Cur/copolymer matrix. After cooling down to room temperature 20 mL of water was added into the resulting matrix and the solution was immediately sonicated three times using a probe-type sonicator (Soniprep 150, Sanyo) under an ice bath at 200 w for 5 min, the power was pulsed for 5 s every 30 s to minimize increases in temperature. The resulting suspension was centrifuged at 4000 rpm for 20 min to remove any aggregated particles and unencapsulated free Cur. The obtained clear supernatant was then lyophilized for 3 days to obtain the Cur-micelles yellow powders.

Evaluation of Particle Size, Size Distribution and Zeta Potential

The average particle size and size distribution of Cur-micelles were determined by dynamic light scattering (DLS) using a Malvern Instrument Zeta Size Nano-S at a detection angle of 173°. Zeta potential was measured using the BC Haven instruments corporation 90 plus particle size analyzer. The samples were dispersed in distilled water at 25 °C and diluted to a suitable density. Each measurement was performed in triplicate.

Determination of Drug-Loading Parameters

The amount of encapsulated Cur in the micelles and the drug loading content were evaluated by direct method.[3] Briefly, 2 mg of lyophilized drug loaded micelles was dissolved in 10 mL acetonitrile to disrupt the micelles structure. The solution was dried under nitrogen, and

then dissolved in mobile phase (acetonitrile/3% acetic acid aqueous solution (75/25, v/v)), centrifuged at a rate of 10000 rpm for 10 minutes and filtered through 0.45 μm filter to obtain a clear solution, then the sample solution was determined at 425 nm by using a Shimadzu HPLC system, equipped with a LC-10 ADvp pump, an SPD-17310 Avp U-vis detector and a Diamonsil C_{18} reversed phase column (4.6 mm $\times$ 250 mm, 5 μm). The column temperature was 30 °C and the flow rate 1.0 mL/min. The encapsulation efficiency and drug loading content were calculated using Eqs. (1) and (2) as follows:

$$\text{Encapsulation efficiency (\%)} = \frac{\text{Weight of Cur in micelles}}{\text{Weight of feeding Cur}} \times 100\% \quad (1)$$

$$\text{Drug loading content (\%)} = \frac{\text{Weight of Cur in micelles}}{\text{Weight of micelles}} \times 100\% \quad (2)$$

X-Ray Diffraction

X-ray diffraction (XRD) spectra of Cur power, empty PAE-*b*-PEG micelles, and Cur loaded PAE-*b*-PEG micelles freeze-dried powders were determined by a Rigaku D/Max 2200/PC diffractometer using a Cu-Kα radiation source (40 kV, 20 mA). The samples were scanned over a 2θ range of 5–45° at a rate of 5 °/min.

In Vitro Cur Release Study

In vitro release behavior of Cur from the PAE-*b*-PEG micelles was developed by dialysis method.[26] Briefly, 10 mg Cur-micelles freeze-dried powders were dispersed in 3 ml PBS (0.01 M, pH 7.4 or pH 5.0) containing 1% v/v of Tween 80 and then placed in a dialysis tube (Snakeskin, Pierce, USA) with a molecular weight cut-off of 3500 Da). The dialysis tube was suspended in 12 mL of release medium and placed in a shaking water bath at 37 °C with a shaking speed of 120 rpm. At predetermined time points, the release medium was completely drawn and replaced with fresh release medium. The amount of Cur in the release medium was determined by HPLC.

Cellular Uptake Study

The cellular uptake of the Cur-micelles by HeLa cells was evaluated by flow cytometer. Cells were seeded at a density of 1.5×10^5 cells/mL (2 mL/well) in 6-well plates and allowed to adhere to the plates for 24 h. The medium was replaced with 200 μL of fresh medium containing curcumin dissolved in DMSO ($\leq$0.1%), or curcumin-loaded micelles at equivalent concentrations of curcumin of 25 μg/mL. At pre-designated time points (0.5, 2, 4, and 24 h after incubation), the cells were washed three times with ice-cold PBS, and then cells were collected by centrifugation and resuspended in 0.5 mL PBS. The amount of micelles uptake was analyzed by a flow cytometer (BD LSRFortessa, Becton Dickinson), after excitation with 405 nm argon lasers and detection with a 515–545 band-pass filter (by detecting the intrinsic fluorescence of Cur which can be excited effectively with the 405 nm laser and showing fluorescence peak at $\sim$520 nm). To study whether the internalization mechanism of micelles into cells through endocytosis pathway, we measured the cellular uptake of Cur-micelles in cold condition (4 °C) versus normal cell culture condition (37 °C).

Confocal Microscopy Imaging

HeLa cells were seeded into glass bottom dishes at 80000 cells per plate in 2 mL of DMEM containing 10% FBS. The dishes were incubated for 4 h at 37 °C in a humidified atmosphere of 95% air and 5% CO_2 and then the medium was replaced with 2 mL of fresh medium containing 25 μg/mL of the Cur-micelles. After the dishes were cultured for 4 h, 100 nM lysotracker red was added to the dishes and incubated for 30 min and then 1 mM of nuclear dye (Hoechst 33342) was added to the dishes and incubated for 10 min. The medium was then removed and washed with PBS and finally replaced with 2 mL PBS. Images were taken using a Leica TCS SP5 microscope. The Lysotracker red was observed at excitation wavelength of 543 nm and the emission wavelength of 580 to 620 nm, the green Cur-micelles were at excitation wavelength of 405 nm and the emission wavelength of 500 nm to 550 nm, the blue nuclear dye was at excitation wavelength of 350 nm and the emission wavelength of 440 nm to 480 nm.

In Vitro Cytotoxicity

The cytotoxicity of the Cur-micelles against HeLa or EMT6 cells was evaluated by MTT assay. Free Cur and the empty PAE-*b*-PEG micelles were used as control. Briefly, HeLa or EMT6 cells were seeded in 96-well plates (5000 cells per well) in 200 μL of DMEM medium and incubated at 37 °C in a 5% CO_2 atmosphere for 24 h. The culture mediums were replaced with 200 μL of fresh mediums containing the Cur-micelles, free Cur or empty PAE-*b*-PEG micelles and incubated for 72 h. Subsequently, 0.1 mL MTT (0.5 mg/mL) was added and incubated for an additional 4 h at 37 °C. The culture medium was then removed from the wells and replaced with DMSO (0.1 mL). The absorbance values were measured at 570 nm by an ELISA plate reader (Varioskan Flash).

Ex Vivo Fluorescence Imaging Experiments

Ex vivo fluorescence imaging experiments were performed using ZKKS-Mulaurora imaging system (Guangzhou Zhongke Kaisheng Medical Technology Co., Ltd., China). The Cur-micelles and free Cur were injected into mice bearing EMT6 tumor via tail vein (at 0.5 mg/kg Cur dose). The mice were sacrificed 2, 6, 12 and 24 h post-injection.

After the major organs or tumors were harvested, the tissues were subjected to fluorescence imaging using ZKKS-Mulaurora imaging system immediately. The ROI (regions of interest) analysis was measured under the assistance of Winmi software.

In Vivo Antitumor Efficacy Evaluation

Female Kumming mice were obtained from SLRC Laboratory Animal Company (Shanghai, China) and used at 6 weeks of age. All animals received care in compliance with the guidelines outlined in the Guide for the Care and Use of Laboratory Animals and all procedures were approved by the Animal Care and Use Committee of Shanghai Jiao Tong University. 0.2 mL EMT6 cells (1.0×10^7 cells/mL) were injected subcutaneously inoculated into female Kumming mice on day 0. On day 5, the tumors had developed to about 300 mm^3, the mice were divided into three groups (6 mice per group) in a way to minimize weight and tumor size differences among the groups. The three groups were intravenously injected with Cur-micelles or free Cur solution (at the Cur does of 10 mg/kg) daily for nine days, respectively. The blank control group was treated with physiological saline. The free Cur solution was prepared as follows: 100 mg of Cur was dissolved in 1 mL of in cremophor EL (polyoxyl 35 castor oil) and dehydrated alcohol (1:1, v/v) solution, and then was diluted with physiological saline to obtain 10 mg/mL free Cur solution. The body weight and tumor size were measured every two days. The tumor volume was calculated using the formula: $V = ab^2/2$, where "a" is the length of the major axis, and "b" is the length of the minor axis. On day 14, the animals were sacrificed by cervical dislocation. The tumor was collected for histopathology and immunohistochemistry analyses. The inhibition rate of tumor growth (IRT) was calculated according to the following formula: IRT = 100% × (mean tumor weight of control group-mean tumor weight of treatment group)/mean tumor weight of control group.

Histological and Immunohistochemical Evaluation of Apoptosis and Proliferation in Tumor

Tumors were collected, fixed paraformaldehyde overnight, and then embedded in paraffin. The paraffin-embedded tumors were cut at 5 μm thickness, and stained with hematoxylin and eosin to assess histological alterations by Olympus BX 51 microscope. Tumor tissue sections were prepared as described above for Ki-67 staining using the labeled streptavidin-biotin method. The primary antibody and secondary antibody were rat anti-mouse monoclonal antibody Ki-67 (Gene Tech) and biotinylated goat anti-rat immunoglobulin (BD Biosciences Pharmingen), respectively. Cellular apoptosis was carried out by reacting sliced tissues with terminal transferase dUTP nick end labeling (TUNEL) assay (Roche) according to the protocol from the manufacturer.

Evaluation of *In Vivo* CD31, VEGF and COX-2 Levels in Tumor Tissues

We studied CD31, vascular endothelial growth factor (VEGF) and cyclooxygenase 2 (COX-2) expressions in the tumor tissue by immunohisto-chemical staining. Briefly, sections of tumors were stained with rat anti-mouse CD31 polyclonal antibody (1:50; BD Pharmingen USA), washed twice with PBS, and followed by incubation with a Cy3-conjugated second antibody (Jackson, USA). For VEGF and COX-2 evaluation, tumor sections were deparaffinaged in xylene. After blocking endogenous peroxidase and nonspecific antibody binding, rabbit polyclonal anti-COX-2 antibody or rabbit polyclonal anti-VEGF antibody was diluted at a ratio of 1:200 in 1% bovine albumin-containing PBS and the tumor sections were incubated for 1 h at room temperature. Staining was performed using avidin-biotin reagents, 3,3-diaminobenzidine, and hydrogen peroxide. A secondary biotinylated antimouse antibody was added, followed by diaminobenzidine as a chromogen. The sections were lightly counterstained with hematoxylin and examined under light microscopy at ×400 magnifications.

Safety Evaluation

To study the toxic effects of the Cur-micelles, 0.2 mL EMT6 cells (1.0×10^7 cells/mL) were injected subcutaneously inoculated into 5∼6 week old female Kumming mice. After 5 days, the tumors had developed to about 300 mm^3, the mice were divided into three groups (6 mice per group) in a way to minimize weight and tumor size differences among the groups. The mice were treated with free Cur (dosage: 10 mg/kg), Cur-micelles (Cur dosage: 10 mg/kg) and physiological saline, respectively via tail vein injection daily for nine days. Blood and serum samples and major organs were collected at 24 h after the last administration for hematologic and histochemistry analysis. Blood was collected in tubes containing Ethylenediamine-N,N,N',N'-tetraacetic acid dipotassium salt (EDTA-2K) and white blood cell (WBC), red blood cell (RBC) and platelet (PLT) were measured by Advia 2120 Automated Hematology Analyzer (Siemens Ltd., Germany). The blood samples were collected into a tube, allowed to stand for 30 min at room temperature and then centrifuged at 4000 rpm for 10 min at 4 °C to collect serum. The serum aspartate transanimase (AST), alanine transaminase (ALT), total bilirubin (T-BIL), ureanitrogen (BUN) and creatinine (CRE) levels were assayed using Hitachi 7600-020 Chemistry Analyzer (Hitachi Ltd., Japan). For histological examinations, specimens of major organs such as heart, liver, spleen and kidney were fixed in 10% phosphate buffered formalin, embedded in paraffin,

sectioned and stained with hematoxylin and eosin (H&E) and photographed under an Olympus BX 51 microscope.

Statistical Analyses

All the experimental data were expressed as means ± standard deviation (SD). Statistical analyses were performed using a student's *t*-tests. The significance of differences between groups considered as $P < 0.05$ and very significant for $P < 0.01$.

RESULTS AND DISCUSSION

Characterization of Cur-Micelles

For effective passive cancer targeting, the size of the drug nanocarrier is of critical importance. It should be normally with the range of 8–200 nm (greater than the renal clearance threshold, ~8 nm, for extended blood circulation time,[28] and the average gap of the leaking blood vessels in cancer tumours, ~200 nm for efficient accumulation inside tumours via the EPR effect.[29] Moreover, they should also evade detection and destruction by the reticuloendothelial system, to achieve longevity during systemic circulation.[30] In this study, the hydrodynamic sizes of the Cur-micelles were determined by DLS as 91.8 ± 1.0 nm (Fig. 1(A)), suggesting it can accumulate readily inside tumors through the EPR effect.[31] The micelles presented a unimodal size distribution with a small polydispersity index of 0.144 ± 0.058, implying a relatively narrow size distribution. The Zeta potential of micelles was measured as −12.5 ± 1.1 mv, indicating that micelles presented negative surface charges. A negative zeta potential is attractive for drug delivery because it can reduce non-specific interactions with blood components which are negative. Moreover, TEM micrograph showed the Cur-micelles were spherical and the size distribution was moderately uniform (Fig. 1(B)).

The Cur content of the Cur loaded PAE-*b*-PEG micelles was estimated as 7.6 ± 0.1% and the Cur encapsulation efficiency by the micelles was ~ 80 ± 1%, suggesting a relatively high drug encapsulation efficiency was achieved here. The high drug encapsulation efficiency by the PAE-*b*-PEG micelles was attributed to a relatively high lipophilicity of Cur and a strong hydrophobic core formed in the polymer micelles.

In addition to size, the status of incorporated drug in micelles is very important for a drug delivery system.[32]

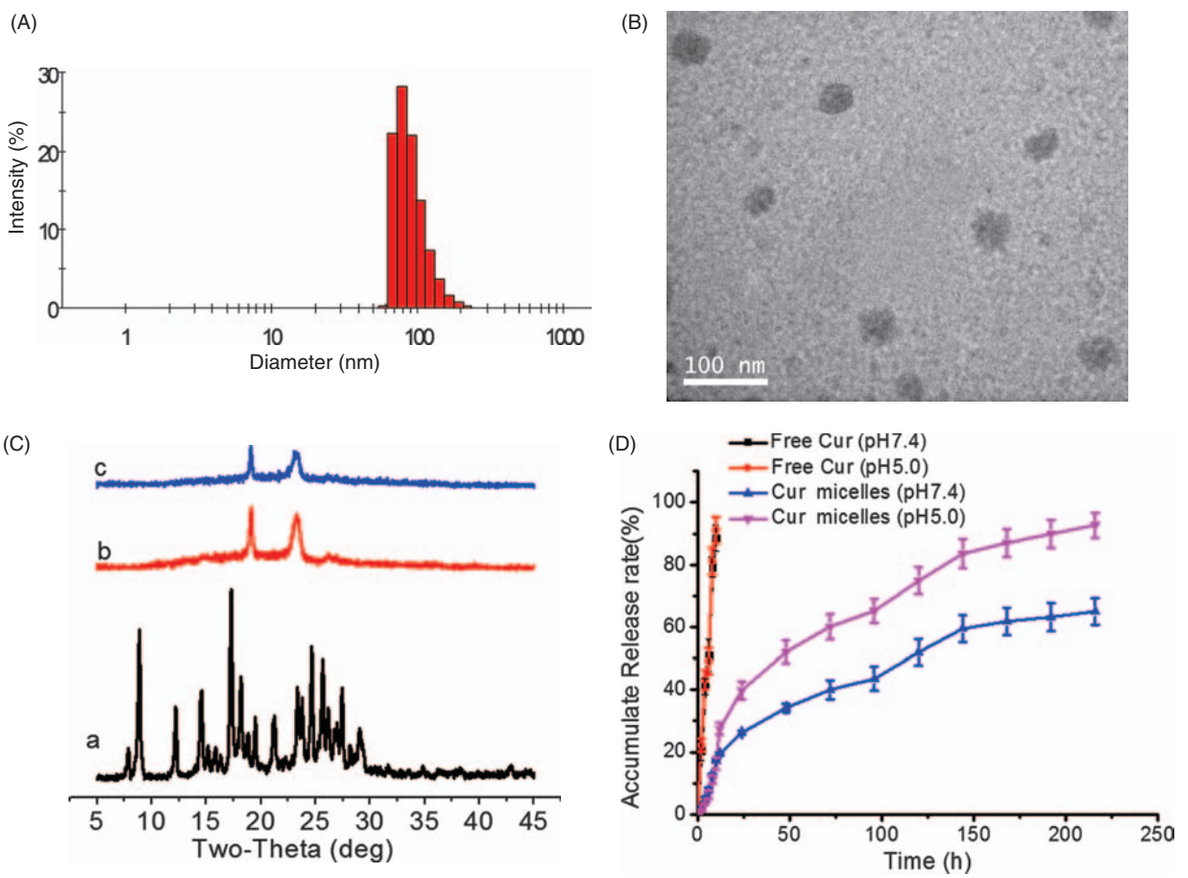

Figure 1. Characteristics of the Cur-micelles. (A) The hydrodynamic diameters of the Cur-micelles by DLS; (B) TEM images of the micelles; (C) XRD spectra of free Cur (a), blank micelles (b), Cur-micelles (c); (D) *In vitro* Cur release profiles of free Cur and the Cur-micelles at pH 7.4 or 5.0, data as mean ± SD, $n = 3$.

Therefore, powder X-ray diffraction (XRD) analysis was performed on the Cur-micelles to examine the crystallinity of the encapsulated Cur. The black, red and blues lines in Figure 1(C) presented the XRD spectra of the Cur powders, empty micelles and freeze-dried Cur-micelles powders, respectively. All of the characteristic diffraction peaks of Cur were absent in the XRD spectrum of the Cur-micelles, indicating that Cur was encapsulated amorphously within the micelles.

In Vitro Cur Released From PAE-*b*-PEG Micelles

In this study, pH 7.4 and 5.0 phosphate buffer solutions were selected to simulate the natural environment of blood and lysosome, respectively. The release profiles of free Cur and the Cur-micelles are showed in Figure 1(D). Free Cur was found to be released rapidly from the dialysis tube into the buffer at both pHs, suggesting that can Cur pass through the dialysis membrane readily into buffer solution. In contrast, the release of Cur from the PAE-*b*-PEG micelles happened more slowly and exhibited a biphasic pattern. After an initial rapid release for the first 12 h, the release rate of Cur slowed down considerably and became steady. The initial rapid release phase may be due to release of drugs deposited at the micelles interface via diffusion, while the slower and sustained release at later stages may be attributed to the degradation/erosion of polymeric matrix.[33]

It is well-known that the cellular uptake of nanoscale objects such as polymer micelles here are mainly via endocytosis, where as a result of the natural endosomal maturation process, the pH of the intracellular vesicles gradually become more and more acidic, reaching ~pH 4–5 in lysosomes. As a result, the different environmental pH may cause significant changes on the drug release behavior.[34] We therefore have also examined the release profiles of Cur-micelles at acidic pH (e.g., 5.0). Figure 1(D) show that the release Cur at normal physiological pH (7.4) was relatively slow and steady, where 65% of the drugs were accumulatively released within 9 days. In contrast, Cur release was faster at pH 5.0, the simulated acidic environment of lysosome, where nearly 100% of the drug content was released after 9 days. This is because the ester and anhydride bonds of PAE-PEG in the Cur-micelles are more easily hydrolyzed at pH 5.0 than 7.4. There are many ester and anhydride bonds in a PAE-PEG molecule. The hydrolysis of PAE would lead to disruption of PAE hydrophobic core of the Cur-micelles and promote drug release.

Cellular Uptake and Intracellular Distribution of the Cur-Micelles

Cur has intrinsic green fluorescence and thus it is highly convenient to monitor the cellular uptake of the Cur-micelles by fluorescence. Endocytosis, a general entry mechanism for macromolecules, is an adenosine triphosphate (ATP)-dependent process which is attenuated down at low temperatures.[35] To assess whether the Cur-micelles entered cells via endocytosis, HeLa cells were incubated with the Cur-micelles for various periods at 4 or 37 °C, and the fluorescence intensity of cells after exposure to micelles was analyzed by flow cytometer. Figure 2 revealed that the fluorescence intensity of the Cur-micelles treated HeLa cells increased steady in a time-dependent manner at 37 °C. While those treated at 4 °C showed much lower fluorescence (~15% that of cells treated at 37 °C after 24 h), suggesting the cell uptake of the Cur-micelles were greatly inhibited. This result is consistent with the Cur-micelles being taken up by HeLa cells mainly via endocytosis route.

Confocal fluorescent microcopy was used to further characterize the cell uptake behavior and to investigate the intracellular distribution of the Cur-micelles (Fig. 3). Significantly higher intracellular fluorescence intensity (green spot) was observed after 4 h incubation with the Cur-micelles in HeLa cells (Fig. 3(a)), which was consistent with the cellular uptake behavior observed by flow cytometry. To further investigate the internalization behavior of the Cur-micelles, confocal fluorescence microscopic images were acquired following lysosome and nucleus staining. Lysosome staining was performed with lysotracker red (Fig. 3(b)) and nucleus staining was performed with Hoechst 33342 (Fig. 3(c)). Overlap of the image of the Cur-micelles channel with that of the Lysotracker red channel produced yellow spots (Fig. 3(d)), indicating some Cur was located in lysosomes after 4 h incubation, implying that the Cur-micelles enter into the HeLa cells through endocytosis. Overlap of the image of the Cur-micelles channel with that of the nucleus channel produced cyan spots (Fig. 3(e)), indicating some Cur was located in nucleus after 4 h incubation. Overlapped image of the Cur-micelles, the Lysotracker and the nucleus channels was shown in (Fig. 3(f)). The intracellular distribution of Cur after incubation with Cur-micelles was significantly different from that of Cur only, which was reported primarily to

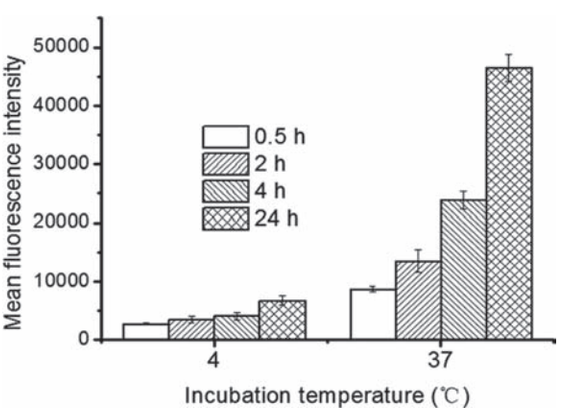

Figure 2. Mean fluorescence intensity of HeLa cells after 0.5, 2, 4, 24 hours incubation with the Cur-micelles at 4 or 37 °C.

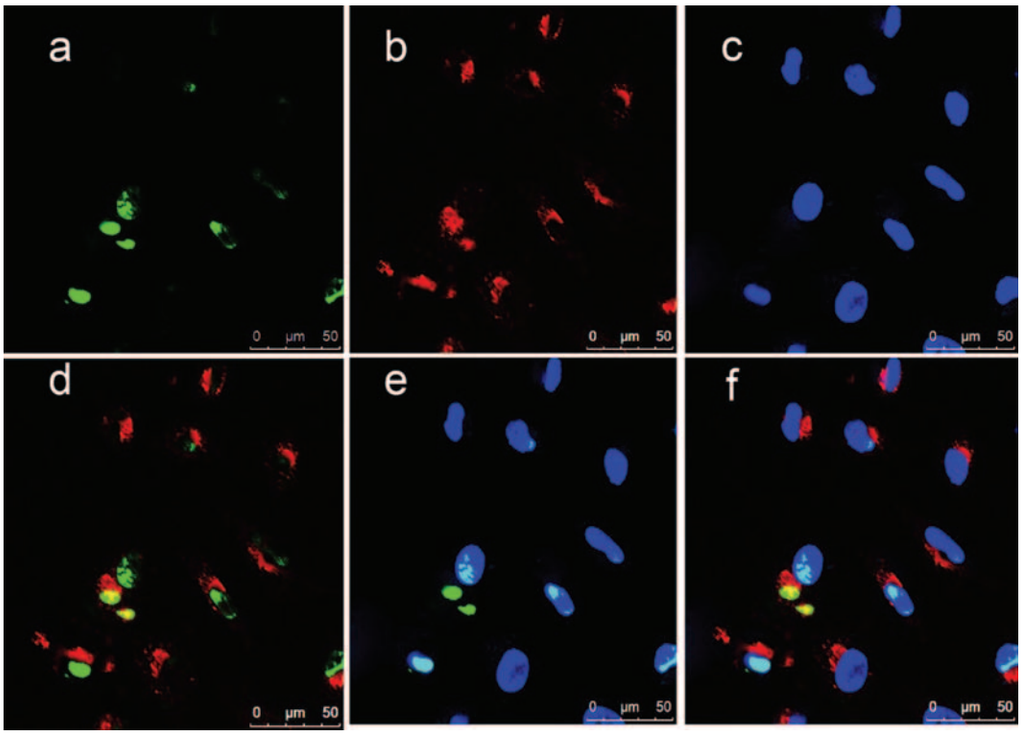

Figure 3. Intracellular distribution of Cur-micelles observed by confocal microscopy. HeLa cells were treated with micelles for 4 h. Images were taken from the micelles channel ((a), green), the lysotracker channel ((b) red), the nuclear dye channel ((c), blue), overlapped of Cur-micelles channel and the lysotracker channel (d), overlapped of Cur-micelles channel and the nuclear dye channel (e), and overlapped of three channels (f).

be localized in the cell membrane and nucleus due to its lipophilic properties.[36, 37]

In Vitro Cytotoxicity

Curcumin is a universal anticancer agent capable of suppressing many types of cancers, including cervical, breast, lung, colorectal, pancreatic and prostate carcinomas. HeLa (cervical cancer) and EMT6 (breast cancer) cell lines were selected to evaluate the cytotoxicities of the Cur-micelles and free Cur. Both cells maintained $> 90\%$ viabilities after being treated with the empty PAE-*b*-PEG micelles over 0.1 to 2000 μg/mL range (data not shown), suggesting that the empty PAE-*b*-PEG micelles are of no-/low-cytotoxicity at such concentrations. In contrast, dose-dependent cytotoxicities were observed for both the Cur-micelles and free Cur treated HeLa or EMT6 cells (Fig. 4). As shown in Table I, the IC_{50} values of free Cur against HeLa cells were 30 ± 2, 27 ± 4, and 26 ± 5 μg/mL for 24, 48, and 72 h incubations, respectively, while those for Cur-micelles were 27 ± 3, 18 ± 3, and 12 ± 3 μg/mL under such conditions. The IC_{50} value of free Cur against HeLa cell decreased slightly ($\sim 13\%$) as the incubation time was increased from 12 to 72 h, in contrast, the IC_{50} value of the Cur-micelles decreased more significantly ($\sim 56\%$) under such prolonged incubations. A similar trend was also observed for EMT6 cells. These results clearly demonstrate that encapsulation of Cur inside the block copolymer micelles could enhance its cytotoxicity significantly.

Biodistribution of Cur-Micelles

Biodistribution of the Cur-micelles in EMT6 tumor bearing Kunming mice was further monitored by fluorescence imaging of isolated visceral organs (heart, liver, spleen, lung and kidney) and tumors after 2, 6, 12 and 24 h post-injection (Fig. 5). We also performed regions of interest (ROIs) analysis on the *ex vivo* fluorescence images to semiquantitatively illustrate the biodistribution information using the Winmi software. The photon numbers per unit area (average signals) of four different parts of the isolated visceral organs and tumors were collected and shown in Figure 6. Free Cur was found to be predominately distributed in liver and kidney, with trace amounts in other organs such as heart, spleen and lung, suggesting that Cur was mainly captured and metabolized by liver. Minor amount of Cur was also found at the tumor target site, which showed a moderate increase during the first 6 h of post intravenous administration, but the amount decreased rapidly thereafter, reaching trace level after 24 h. This result indicates that like most other small-molecule drugs, Cur has a relatively short blood circulation and rapid renal clearance, most likely due to its small ($<$ renal clearance

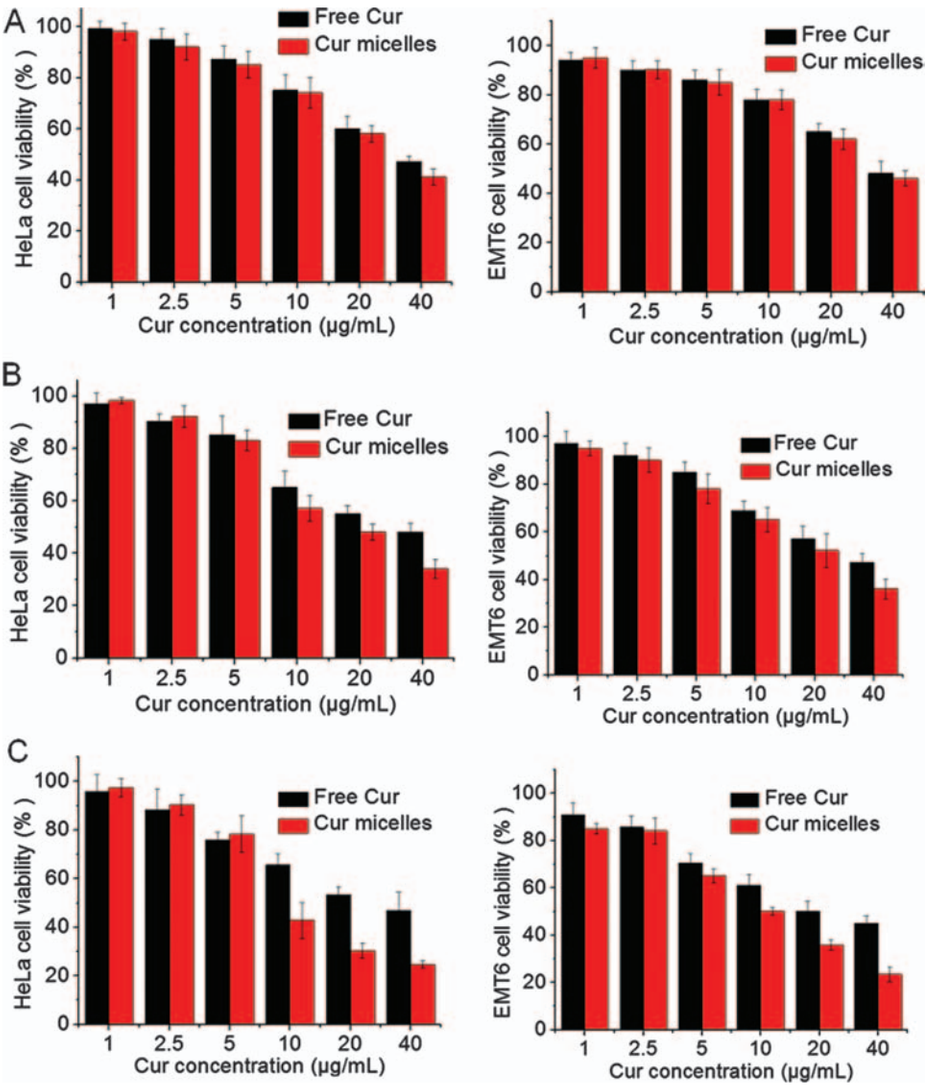

Figure 4. **Cytotoxicities of the Cur-micelles against HeLa cells or EMT6 cells after incubation for 24 h (A), 48 h (B), or 72 h (C), data are presented as mean ± SD ($n = 10$).**

threshold ~ 8 nm) sizes,[28] which can limit the longility of treatment efficacy.

For Cur-micelles injected mice (identical Cur dose), the Cur amounts at both the liver and kidney were considerably less, but significantly more at the target tumor site compared to free Cur treated ones. More importantly, the Cur fluorescence progressively increased over the whole 24 h monitoring period for the Cur-micelles treated mice, presumably due to a much longer blood circulation time afforded by the nano-encapsulation, allowing the Cur-micelles to be effectively accumulated at the tumor site via its characteristic EPR effect. These results indicated that micelle encapsulation completely changed the pharmakinetics and biodistribution of the Cur. Importantly, at 24 h post administration, the Cur concentration at the tumor site for Cur-micelle injected mice was ~ 16 times higher than that treated with free Cur, demonstrating that the Cur-micelles are much more efficient in delivering Cur to the tumor. Moreover, the Cur-micelles showed less RES uptake and more tumor accumulation than free Cur, which is attributed to the stealth effect of PEGylated well-controlled particle surface.[38] These, together with the observation of lower amount of Cur being distributed in

Table I. **The IC_{50} values (μg/mL) of various preparations of Cur against two kinds of tumor cells for 24, 48 and 72 h. Data as mean ± SD ($n = 3$).**

Cell	Preparations	24 h	48 h	72 h
HeLa	Free Cur	30 ± 2	27 ± 4	26 ± 5
	Cur micelles	27 ± 3	18 ± 3	12 ± 3
EMT6	Free Cur	27 ± 4	24 ± 5	23 ± 4
	Cur micelles	25 ± 3	19 ± 2	11 ± 5

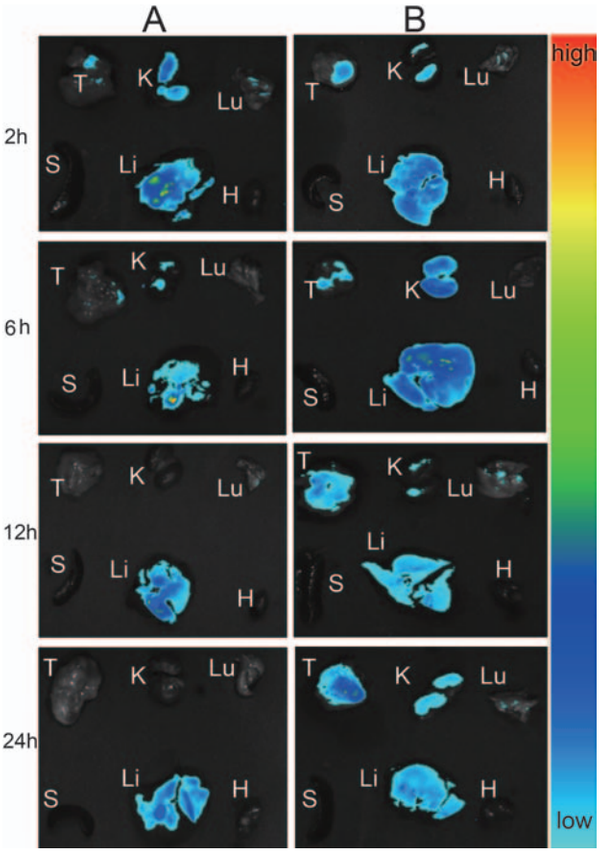

Figure 5. **Representative fluorescence images of tumor and organs harvested from Kunming mice bearing EMT6 tumor 2, 6, 12 and 24 h after intravenous injection of (A) free Cur and (B) Cur-micelles.**

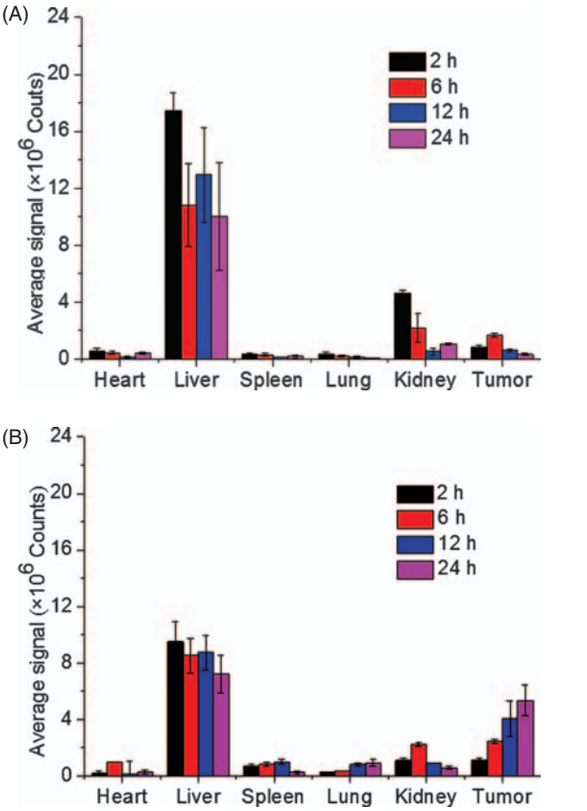

Figure 6. **Cur relative amounts (expressed as average signals) in organs (heart, liver, spleen, lung and kidney) and tumor of Kunming mice bearing EMT6 tumor after 2, 6, 12 and 24 hours post i.v. injection of Cur solution at a dose of 0.5 mg/kg (A) and the Cur-micelles solution at an equivalent Cur dose of 0.5 mg/kg (B).**

other key organs, suggest that the Cur-micelle formulation can offer more effective, targeted cancer treatment with significantly reduced toxic side-effects compared with the free drug on its own.

In Vivo Anticancer Efficacy

The *in vivo* antitumor activity of the Cur-micelle was evaluated on an EMT6 tumor model. Mice bearing the tumors were intravenously administered with normal saline, free Cur (10 mg/kg) and the Cur-micelle (10 mg/kg equivalent Cur for micelle), respectively. Figure 7(A) shows the tumor size changes after the therapy. The Cur micelles-treated group resulted in smaller tumor volume than either the Cur-treated group or the control group ($p < 0.01$). On day 13, tumor volumes of the Cur and Cur-micelle treated mice groups were $59\% \pm 6\%$ and $40\% \pm 5\%$ of that of the control group, respectively. At the end of this *in vivo* experiment, the tumors of all different groups were removed, photographed and weighted. The tumor sizes from Cur micelle-treated group were obviously smaller than those treated with free Cur and saline control groups (Fig. 7(C)), which agreed well with the relative tumor volume results shown in Figure 7(A). Moreover, the tumor weights in mice treated with the Cur-micelle were considerably lower compared to the free Cur ($p < 0.01$) and saline control groups ($p < 0.01$) (Fig. 7(D)). Accordingly, the inhibition rates of tumor growth by free Cur and Cur-micelle on the EMT6 tumors were therefore estimated as $\sim 32\%$ and $\sim 60\%$, respectively. This result agrees well with the biodistribution studies, where the Cur-micelle showed enhanced Cur-accumulation inside the tumor site compared to free Cur, and hence providing a higher therapeutic efficacy. The body weights of all of the mice gradually increased throughout the experiments (Fig. 7(B)) and no behavioral abnormalities were observed during the course of therapy in all groups, indicating that the treatments did not cause severe side-effects. This *in vivo* study results clearly demonstrated that:

(1) systemic application of the Cur-micelles can significantly inhibit the growth of subcutaneous EMT6 tumors *in vivo*;

(2) encapsulation of Cur in the PAE-*b*-PEG micelle can enhance its *in vivo* anticancer activity;

(3) both Cur and Cur-micelles did not cause severe side effects on preclinical mouse models.

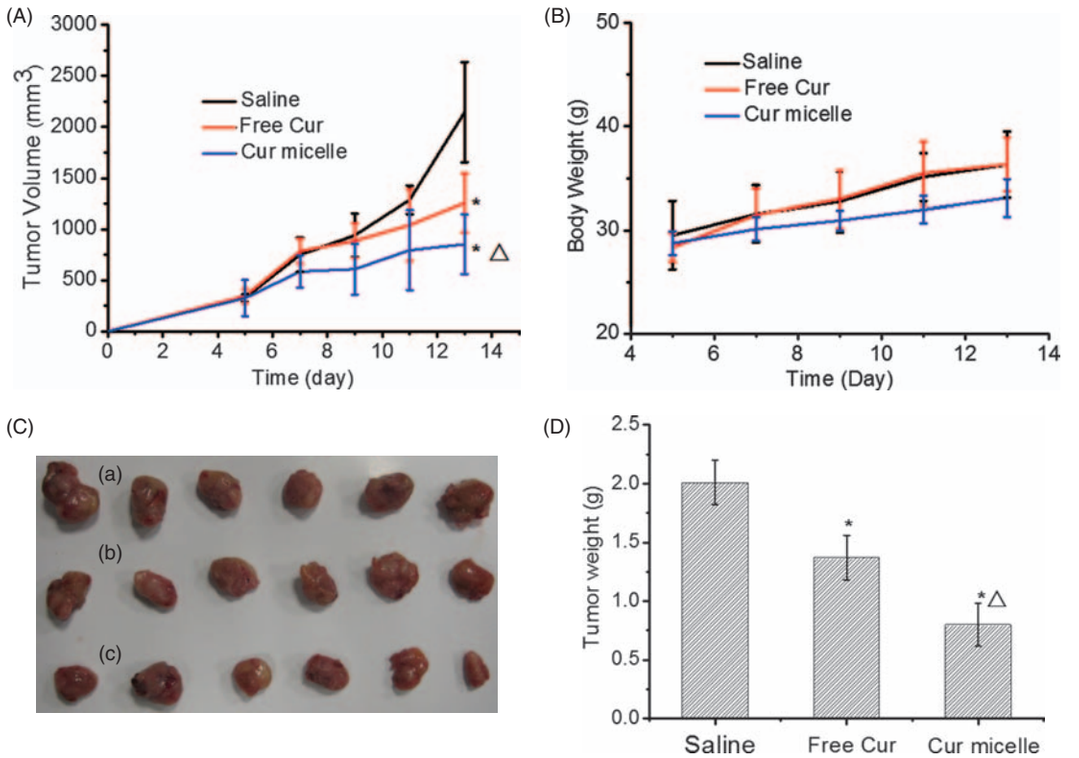

Figure 7. **Changes of tumor and body weights of Kunming mice bearing EMT6 tumor with time. 0.2 mL EMT6 cells (1.0×10^7 cells/mL) were injected subcutaneously inoculated into female Kumming mice on day 0. On day 5, the mice were divided into three groups (6 mice per group) and intravenously injected with the Cur-micelles solution (an equivalent Cur dose of 10 mg/kg), free Cur solution (a dose of 10 mg/kg), saline as negative control daily for nine days, respectively. (A) Tumor volume vs. time, $^*p < 0.01$, compared to control; $\Delta p < 0.01$, compared to free Cur; (B) Body weights versus time; (C) photos of tumors after 9 days injection with saline (a), free curcumin (b), or the Cur-micelles (c); (D) Tumor weights after 9 days injection with the Cur-micelles, free Cur or saline, (significant difference, $^*p < 0.01$, compared to control; $\Delta p < 0.01$, compared to free Cur).**

Apoptosis and Proliferation in Tumor

To further evaluate the antitumor efficacy, the tumors after treatment with saline, free Cur and Cur-micelles were excised from the mice and sectioned for pathology and immuno-histochemical analysis. As presented in Figure 8, tumor cells with a large nucleus and a spherical or spindle shape were observed in the saline control tumor tissue. However, various degree of tissue necrosis was observed, chromatin was concentrated and distributed around the edge, and nuclei became pyknotic or absence, in the free Cur- and Cur micelle-treated groups at 10 mg/kg. The necrosis area in the Cur-micelles group was the largest among the tested groups. The terminal deoxynucleotidyl ransferase-mediated dUTP nick-end labeling (TUNEL) assay was further used to detect DNA fragmentation, a marker of late apoptosis in nuclei of tumor cells. In line with the above hematoxylin and eosin (H&E) observation, more apoptotic tumor cells were found in the Cur micelle- and free Cur treated groups compared with the saline control group, and the Cur micelles-treated group showed a more pronounced apoptosis induction effect than the free Cur group.

We have further analyzed the activity of the Cur-micelles on proliferation of tumor cells by immunohistochemical staining of Ki-67. Within a similar high power field (400×), more Ki-67 negative cells in tumor tissues were observed in Cur micelle-treated mice compared with those of free Cur or saline control group. Taken together, these results clearly indicated that the Cur-micelles provided a higher therapeutic efficacy compared with free Cur, which was consistent with the *in vivo* antitumor efficacy and Cur biodistribution results described in previous sections. This further confirms that the Cur-micelles can deliver more Cur into the tumor target presumably via its characteristic EPR effect, and thus enhancing the anti-tumor efficacy of Cur.

Anti-Angiogenesis Effect of Cur-Micelles

Angiogenesis, the formation of new vessels, has a major role in tumor growth, dissemination and metastasis in both solid and hematological tumors.[39] Immunohistochemical assessment can be utilized for investigation of tumor vessels in tumor tissue.[40] In this regard, tumors from the mice of different experimental groups were excised

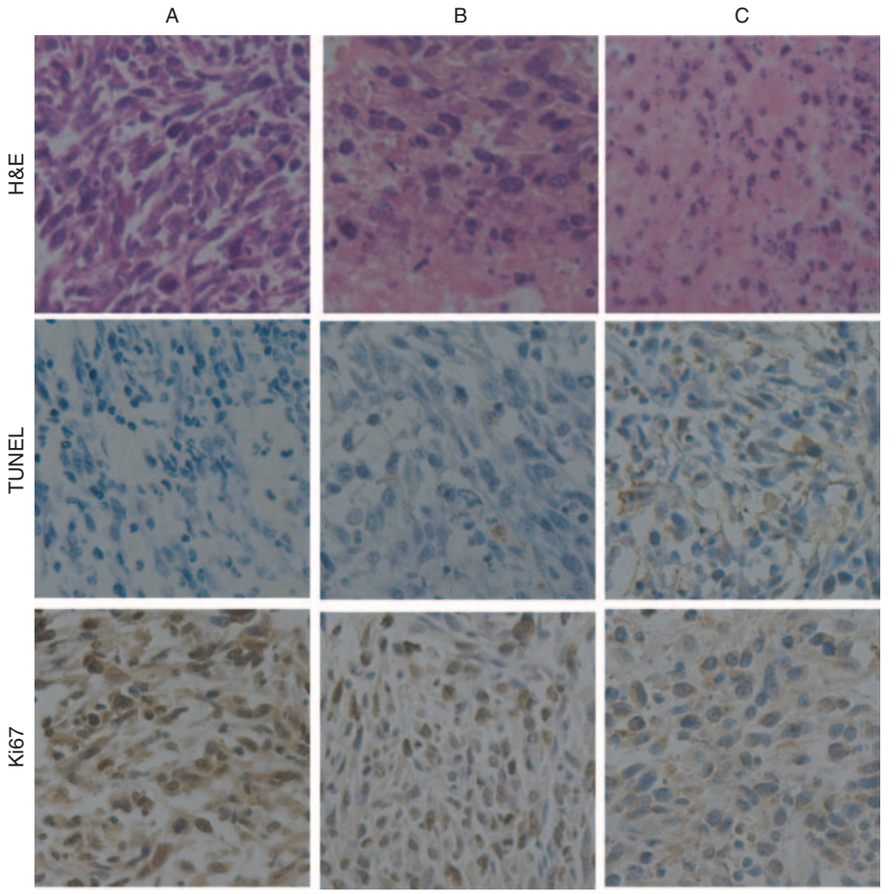

Figure 8. **H. E., TUNEL and Ki-67 photographs of Tumor tissue of Kunming mice bearing EMT6 tumor after 9 days i.v. injection with saline (A) as negative control, free Cur at a dose of 10 mg/kg (B) and the Cur-micelles at an equivalent Cur dose of 10 mg/kg (C).**

and sectioned for immunohistochemical analysis. The microvessel density in the tumors from different groups was examined using a CD31 staining method.[40] As shown in Figure 9, microvessels were clearly observable after CD31 staining labeled with a Cy3 fluorophore. Figure 9 (top panel) showed that considerable amount of microvessels were clearly observed in the Cur treated and saline control groups (shown in red fluorescence). In contrast, few microvessels were observed in the Cur-micelle treated group, confirming that the Cur-micelles have significant inhibition toward microvessel formation in tumors.

As VEGF is a major proangiogenesis factor in tumor microenvironment and COX-2 is involved in the regulation of VEGF-induced angiogenesis.[41, 42] So, we also tested the VEGF and COX-2 expression level in tumor tissue after different treatments. Figure 9 revealed that the VEGF and COX-2 expression levels were significantly inhibited in the Cur-micelles treated group, while the free Cur treated and saline control groups showed much less inhibition on VEGF and COX-2 expression. These results clearly indicated that tumor angiogenesis was significantly inhibited by treatment with the Cur-micelles, which is key to tumor growth and metastasis. The produced antiangiogenic effects could reduce the blood supply to the tumor and suppressing tumor growth *in vivo*. The enhanced anti-angiogenesis effect for the Cur-micelles here is consistent with its much higher antitumor activities shown in tumor volume (Fig. 7(A)) and weight (Fig. 7(D)) growth curves. The higher antiangiogenic effects produced by the Cur-micelles are also consistent with the significantly enhanced Cur accumulation in tumor observed in Figure 5.

Safety Evaluation

The viabilities of HeLa and EMT6 cells following 72 hours of continuous exposure to Cur-free empty PAE-*b*-PEG micelles at different concentration were measured by MTT assay. The empty micelles were found to be not toxic to these cells at concentrations up to 2 mg/mL, confirming that the anticancer effects observed above were not originated from the PAE-*b*-PEG micelles but the loaded Cur drug. This again verifies the excellent the biocompatibility and non-toxicity of the block copolymer. Clinical trials have proven that Cur is safe for humans even at a high dose of 12 g per day.[43–44] However, for any new drug nanoformulation (nanomedicine), one potential problem is its biosafety, because they have completely

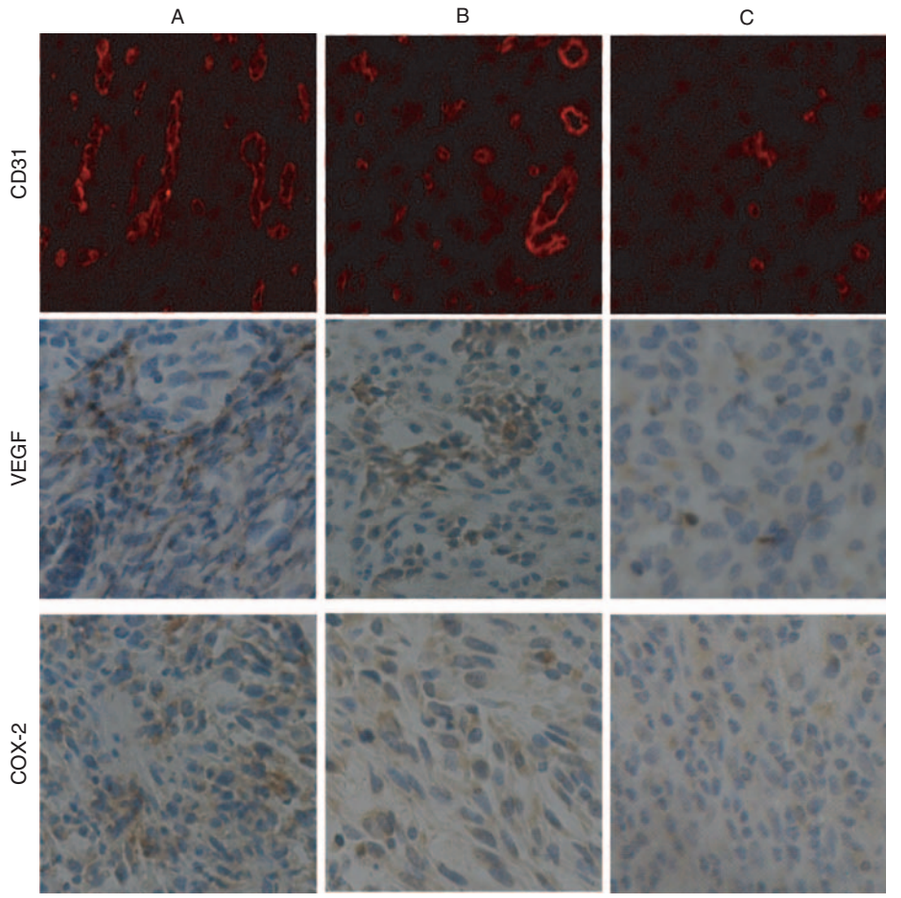

Figure 9. **CD31, VEGF and COX-2 photographs of Tumor tissue of Kunming mice bearing EMT6 tumor after 9 days i.v. injection with saline (A) as negative control, free Cur at a dose of 10 mg/kg (B) and the Cur-micelles at an equivalent Cur dose of 10 mg/kg (C).**

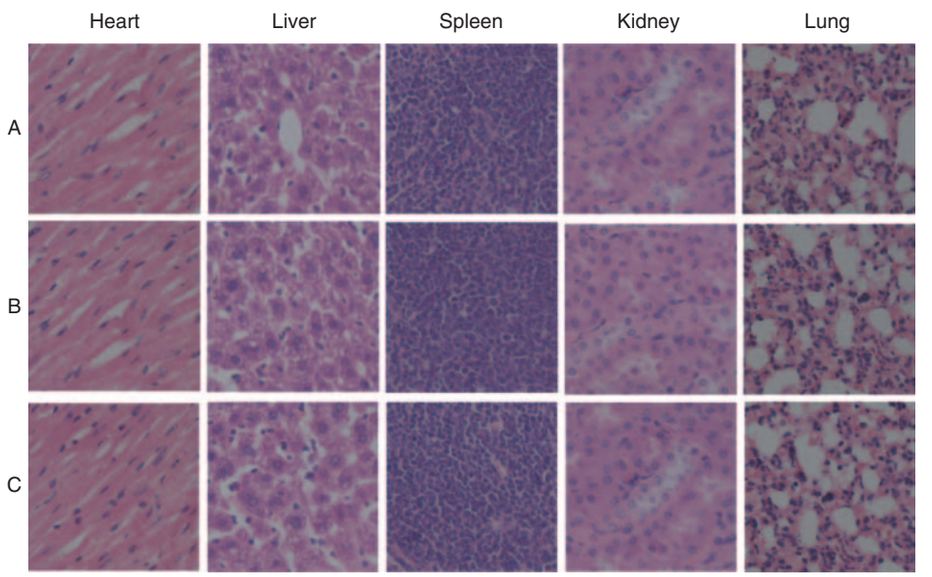

Figure 10. **H.E. photographs of heart, liver, spleen, lung and kidney of Kunming mice bearing EMT6 tumor after 9 days i.v. injection with saline (A) as negative control, free Cur at a dose of 10 mg/kg (B) and the Cur-micelles at an equivalent Cur dose of 10 mg/kg (C).**

different pharmakinetics and biodistribution properties.[45] Thus, *in vivo* toxicity should be evaluated to prove their *in vivo* safety. As a result, we also evaluated the *in vivo* systematic toxicity of the Cur-micelles with Kunming mice bearing EMT6 tumors against free Cur and saline controls. Compared with the saline control group, no deaths and serious body weight loss were observed in all test groups during the study period (data not shown). To evaluate the acute toxicity of major organs caused by the Cur-micelles, heart, liver, spleen, lung and kidney collected 24 h after the last administration were stained with hematoxylin and eosin (H&E). As shown in Figure 10, all of the organs revealed no obvious histopathological abnormalities, degeneration, lesions or necrosis in all groups. The results indicated that no visible inflammatory response and lesions in the organs were caused by Cur-micelle treatment.

It is well known that most of the intravenously injected nanoparticles are taken up and eliminated by mononuclear phagocyte system (MPS), including liver and kidney tissue.[46] Moreover, from the biodistribution assay, the Cur-micelles were abundant in the liver and kidney tissue. Thus, potential pathological lesions in liver and kidney induced by Cur-micelles can be characterized by an increase in biochemical parameters including the liver function marker alanine aminotransferase (ALT), aspartate aminotransferase (AST), and total bilirubin (T-Bil), and the kidney function markers such as creatinine (CRE) and blood urea nitrogen (BUN). The measured hematological parameters for studied groups are shown in Table II. All of the measured biochemical parameters in the Cur-micelle treated group showed no statistically significant difference from the free Cur and saline control groups, indicating that multiple dosing of the Cur-micelles had minimal impact on the function of liver and kidney.

To further investigate any potential toxic effect of the Cur-micelles on the treated mice, hematology analysis was carried out. The important hematology markers such as white blood cell (WBC), red blood cell (RBC) and platelet count are shown in Table III. Similarly, there was no significant difference in any of tested hematology parameters among the Cur-micelles, free Cur and saline groups. All these aforementioned results demonstrate that successive daily intravenous administration of 10 mg/kg Cur-micelles for nine days did not cause acute toxicity to the major organs and hematological system in mice. Therefore the Cur-micelle developed herein appears to be a safe, highly attractive nanomedicine that can be used for effective, targeted treatment of cancer without any significant side effects.

Table II. Serum biochemical levels of mice after i.v. injection of Cur solution at a dose of 10 mg/kg or Cur micelles solution at an equivalent Cur dose of 10 mg/kg daily for nine days.

Groups	ALT (U/L)	AST (U/L)	T-Bil (μmol/L)	BUN (mmol/L)	CRE (μmol/L)
Saline	27.1 ± 2.3	122.3 ± 8.9	3.2 ± 0.4	8.47 ± 0.57	95.3 ± 3.2
Free Cur	28.3 ± 3.9	122.4 ± 10.1	3.0 ± 0.5	8.41 ± 1.07	96.0 ± 4.6
Cur micelles	28.1 ± 3.3	121.1 ± 12.5	2.9 ± 0.4	8.66 ± 0.60	96.7 ± 5.5

Table III. Mice blood cell counts after i.v. injection of Cur solution at a dose of 10 mg/kg or Cur micelles solution at an equivalent Cur dose of 10 mg/kg daily for nine days.

Groups	WBC ($\times 10^9$/L)	RBC ($\times 10^{12}$/L)	Platelets ($\times 10^9$/L)
Saline	5.59 ± 1.08	8.16 ± 2.01	517 ± 136
Free Cur	5.25 ± 1.43	7.95 ± 1.79	502 ± 160
Cur micelle	5.03 ± 1.89	7.86 ± 1.05	528 ± 150

CONCLUSION

In summary, we have developed a novel, stable Cur based nanomedicine by encapsulation of Cur into PAE-*b*-PEG micelles, overcoming a major problem of poor drug water solubility. The Cur-micelles offer pH-dependent (faster at lower pH), sustained Cur release which is advantageous for drug delivery. *In vitro* cell viability studies using HeLa and EMT6 cancer cell models revealed that the Cur-micelles is more cytotoxic than free Cur. Moreover, *in vivo* preclinical evaluation using EMT6 tumor-bearing mouse models revealed that the Cur-micelles can significantly increase the amount of Cur being delivered into target cancer tumor, resulting in significantly enhanced inhibition of tumor growth and anti-angiogenesis effects compared to free Cur. Preliminary *in vivo* safety tests revealed no subacute toxicity to hematological system, major organs or tissues in mice for successive intravenous administration of the Cur-micelles. Taken together, we believe the Cur loaded PAE-*b*-PEG micelle has excellent potential to be developed into a safe, targeted nanomedicine for effective cancer chemotherapy. Currently, we are focused on further optimization and preclinical evaluation of the Cur-micelle systems, investigating the dose-response relationship and long-term *in vivo* safety.

Acknowledgments: This work is supported by National Natural Science Foundation of China (NSFC) (Grant No. 81171439), National Basic Research Program of China (973 Program, Grant 2010CB529902) and The National Key Technology R&D Program of the Ministry of Science and Technology (2012BAI18B01). The authors are grateful to Instrumental Analysis Center of Shanghai Jiao Tong University and Professor Che Shun-Ai for their technical supporting in XRD examinations.

REFERENCES

1. R. K. Maheshwari, A. K. Singh, J. Gaddipati, and R. C. Srimal, Multiple biological activities of curcumin: A short review. *Life Sci.* 78, 2081 (**2006**).
2. S. M. Oliveira, I. F. Amaral, M. A. Barbosa, and C. C. Teixeira, Engineering endochondral bone: *In vitro* studies. *Tissue Eng. Part A* 15, 625 (**2009**).

3. L. Song, Y. Shen, J. Hou, L. Lei, S. Guo, and C. Qian, Polymeric micelles for parenteral delivery of curcumin: Preparation, characterization and *in vitro* evaluation. *Colloid Surf. A-Physicochem. Eng. Asp.* 390, 25 **(2011)**.

4. G. Guo, S. Fu, L. Zhou, H. Liang, M. Fan, F. Luo, Z. Qian, and Y. Wei, Preparation of curcumin loaded poly(epsilon-caprolactone)–poly(ethylene glycol)–poly(epsilon-caprolactone) nanofibers and their *in vitro* antitumor activity against Glioma 9L cells. *Nanoscale* 3, 3825 **(2011)**.

5. M. M. Yallapu, M. Jaggi, and S. C. Chauhan, Curcumin nanoformulations: A future nanomedicine for cancer. *Drug Discov. Today* 17, 71 **(2012)**.

6. F. Akhtar, M. Rizvi, and S. K. Kar, Oral delivery of curcumin bound to chitosan nanoparticles cured Plasmodium yoelii infected mice. *Biotechnol. Adv.* 30, 310 **(2012)**.

7. L. Li, B. Ahmed, K. Mehta, and R. Kurzrock, Liposomal curcumin with and without oxaliplatin: Effects on cell growth, apoptosis, and angiogenesis in colorectal cancer. *Mol. Cancer Ther.* 6, 1276 **(2007)**.

8. C. Gong, S. Deng, Q. Wu, M. Xiang, X. Wei, L. Li, X. Gao, B. Wang, L. Sun, Y. Chen, Y. Li, L. Liu, Z. Qian, and Y. Wei, Improving antiangiogenesis and anti-tumor activity of curcumin by biodegradable polymeric micelles. *Biomaterials* 34, 1413 **(2013)**.

9. M. L. Gou, K. Men, H. S. Shi, M. L. Xiang, J. Zhang, J. Song, J. L. Long, Y. Wan, F. Luo, and X. Zhao, Curcumin-loaded biodegradable polymeric micelles for colon cancer therapy *in vitro* and *in vivo*. *Nanoscale* 3, 1558 **(2011)**.

10. A. Safavy, K. P. Raisch, S. Mantena, L. L. Sanford, S. W. Sham, N. R. Krishna, and J. A. Bonner, Design and development of water-soluble curcumin conjugates as potential anticancer agents. *J. Med. Chem.* 50, 6284 **(2007)**.

11. P. Anand, A. B. Kunnumakkara, R. A. Newman, and B. B. Aggarwal, Bioavailability of curcumin: Problems and promises. *Mol. Pharm.* 4, 807 **(2007)**.

12. A. S. Jain, S. M. Shah, M. S. Nagarsenker, Y. Nikam, R. P. Gude, F. Steiniger, J. Thamm, and A. Fahr, Lipid colloidal carriers for improvement of anticancer activity of orally delivered quercetin: Formulation, characterization and establishing *in vitro in vivo* advantage. *J. Biomed. Nanotechnol.* 9, 1230 **(2013)**.

13. A. L. Miranda-Vilela, R. C. A. Peixoto, J. P. F. Longo, F. A. Portilho, K. L. C. Miranda, P. P. C. Sartoratto, S. N. Bao, R. B. De Azevedo, and Z. G. M. Lacava, Dextran-functionalized magnetic fluid mediating magnetohyperthermia combined with preventive antioxidant pequi-oil supplementation: Potential use against cancer. *J. Biomed. Nanotechnol.* 9, 1261 **(2013)**.

14. K.-J. Lee, J. H. An, J.-R. Chun, K.-H. Chung, W.-Y. Park, J.-S. Shin, D.-H. Kim, and Y. Y. Bahk, *In vitro* analysis of the anti-cancer activity of mitoxantrone loaded on magnetic nanoparticles. *J. Biomed. Nanotechnol.* 9, 1071 **(2013)**.

15. G. Zhang, X. Zeng, and P. Li, nanomaterials in cancer-therapy drug delivery system. *J. Biomed. Nanotechnol.* 9, 741 **(2013)**.

16. C. A. Dehelean, S. Feflea, D. Gheorgheosu, S. Ganta, A. M. Cimpean, D. Muntean, and M. M. Amiji, Anti-angiogenic and anticancer evaluation of betulin nanoemulsion in chicken chorioallantoic membrane and skin carcinoma in balb/c mice. *J. Biomed. Nanotechnol.* 9, 577 **(2013)**.

17. Q. Long, Y. Xie, Y. Huang, Q. Wu, H. Zhang, S. Xiong, Y. Liu, L. Chen, Y. Wei, and X. Zhao, Induction of apoptosis and inhibition of angiogenesis by pegylated liposomal quercetin in both cisplatin-sensitive and cisplatin-resistant ovarian cancers. *J. Biomed. Nanotechnol.* 9, 965 **(2013)**.

18. M. Sharma, R. Malik, A. Verma, P. Dwivedi, G. S. Banoth, N. Pandey, J. Sarkar, P. R. Mishra, and A. K. Dwivedi, Folic acid conjugated guar gum nanoparticles for targeting methotrexate to colon cancer. *J. Biomed. Nanotechnol.* 9, 96 **(2013)**.

19. A. Gupta, S. Asthana, R. Konwar, and M. Chourasia, An insight into potential of nanoparticles-assisted chemotherapy of cancer using gemcitabine and its fatty acid prodrug: a comparative study. *J. Biomed. Nanotechnol.* 9, 915 **(2013)**.

20. V. Saxena and M. D. Hussain, Polymeric mixed micelles for delivery of curcumin to multidrug resistant ovarian cancer. *J. Biomed. Nanotechnol.* 9, 1146 **(2013)**.

21. M. E. Davis, Nanoparticle therapeutics: An emerging treatment modality for cancer. *Nat. Rev. Drug Discov.* 7, 771 **(2008)**.

22. M. L. Adams, A. Lavasanifar and G. S. Kwon, Amphiphilic block copolymers for drug delivery. *J. Pharm. Sci.* 92, 1343 **(2003)**.

23. Z. He, Y. Yu, Y. Zhang, Y. Yan, Y. Zheng, J. He, Y. Xie, G. He, Y. Wei, and X. Song, Gene delivery with active targeting to ovarian cancer cells mediated by folate receptor. *J. Biomed. Nanotechnol.* 9, 833 **(2013)**.

24. L. Lv, Y. Shen, M. Li, X. Xu, M. Li, S. Guo, and S. Huang, Preparation and *in vitro* evaluation of novel poly(anhydride-ester)-based amphiphilic copolymer curcumin-loaded micelles. *J. Biomed. Nanotechnol*. 10, 1 **(2014).**

25. J. Mönkäre, R. A. Hakala, M. A. Vlasova, A. Huotari, M. Kilpeläinen, A. Kiviniemi, V. Meretoja, K. H. Herzig, H. Korhonen, J. V. Seppälä, and K. Järvinen, Biocompatible photocrosslinked poly(ester anhydride) based on functionalized poly([epsilon]-caprolactone) prepolymer shows surface erosion controlled drug release *in vitro* and *in vivo*. *J. Controlled Release* 146, 349 **(2010)**.

26. R. A. Hakala, H. Korhonen, V. V. Meretoja, and J. V. Seppä Lä, Photo-cross-linked biodegradable poly(ester anhydride) networks prepared from alkenylsuccinic anhydride functionalized poly(ε-caprolactone) precursors. *Biomacromolecules* 12, 2806 **(2011)**.

27. Y. Wang, C. Wang, C. Gong, Y. Wang, G. Guo, F. Luo, and Z. Qian, Polysorbate 80 coated poly(-caprolactone)–poly(ethylene glycol)–poly(-caprolactone) micelles for paclitaxel delivery. *Int. J. Pharm.* 434, 1 **(2012)**.

28. H. S. Choi, W. Liu, P. Misra, E. Tanaka, J. P. Zimmer, B. I. Ipe, M. G. Bawendi, and J. V. Frangioni, Renal clearance of quantum dots. *Nat. Biotechnol.* 25, 1165 **(2007)**.

29. D. Peer, J. M. Karp, S. Hong, O. C. Farokhzad, R. Margalit, and R. Langer, Nanocarriers as an emerging platform for cancer therapy. *Nat. Nanotechnol.* 2, 751 **(2007)**.

30. M. J. Santander-Ortega, N. Csaba, L. González, D. Bastos-González, J. L. Ortega-Vinuesa, and M. J. Alonso, Protein-loaded PLGA-PEO blend nanoparticles: Encapsulation, release and degradation characteristics. *Colloid Polym. Sci.* 288, 141 **(2010)**.

31. H. Xin, X. Jiang, J. Gu, X. Sha, L. Chen, K. Law, Y. Chen, X. Wang, Y. Jiang, and X. Fang, Angiopep-conjugated poly(ethylene glycol)-co-poly([epsilon]-caprolactone) nanoparticles as dual-targeting drug delivery system for brain glioma. *Biomaterials* 32, 4293 **(2011)**.

32. P. L. Soo, L. Luo, D. Maysinger, and A. Eisenberg, Incorporation and release of hydrophobic probes in biocompatible polycaprolactone-block-poly(ethylene oxide) micelles: Implications for drug delivery. *Langmuir* 18, 9996 **(2002)**.

33. R. Misra and S. K. Sahoo, Intracellular trafficking of nuclear localization signal conjugated nanoparticles for cancer therapy. *Eur. J. Pharm. Sci.* 39, 152 **(2010)**.

34. M. Li, W. Song, Z. Tang, S. Lv, L. Lin, H. Sun, Q. Li, Y. Yang, H. Hong, and X. Chen, Nanoscaled poly(l-glutamic acid)/doxorubicin-amphiphile complex as pH-responsive drug delivery system for effective treatment of nonsmall cell lung cancer. *Acs Appl. Mater. Interfaces* 5, 1781 **(2013)**.

35. J. Chang, Y. Li, G. Wang, B. He, and Z. Gu, Fabrication of novel coumarin derivative functionalized polypseudorotaxane micelles for drug delivery. *Nanoscale* 5, 813 **(2013)**.

36. A. Kunwar, A. Barik, B. Mishra, K. Rathinasamy, R. Pandey, and K. Priyadarsini, Quantitative cellular uptake, localization and cytotoxicity of curcumin in normal and tumor cells. *BBA-General Subjects* 1780, 673 **(2008)**.

37. H. Tang, C. J. Murphy, B. Zhang, Y. Shen, E. A. Van Kirk, W. J. Murdoch, and M. Radosz, Curcumin polymers as anticancer conjugates. *Biomaterials* 31, 7139 **(2010)**.

38. S.-D. Li and L. Huang, Stealth nanoparticles: High density but sheddable PEG is a key for tumor targeting. *J. Control. Release* 145, 178 **(2010)**.

39. P. Carmeliet and R. K. Jain, Angiogenesis in cancer and other diseases. *Nature* 407, 249 **(2000)**.

40. S. W. Chung, M. Lee, S. M. Bae, J. Park, O. C. Jeon, H. S. Lee, H. Choe, H. S. Kim, B. S. Lee, and R.-W. Park, Potentiation of anti-angiogenic activity of heparin by blocking the ATIII-interacting pentasaccharide unit and increasing net anionic charge. *Biomaterials* 35, 9070 **(2012)**.

41. J. Duan, Y. Zhang, S. Han, Y. Chen, B. Li, M. Liao, W. Chen, X. Deng, J. Zhao, and B. Huang, Synthesis and *in vitro*/*in vivo* anticancer evaluation of curcumin-loaded chitosan/poly(butyl cyanoacrylate) nanoparticles. *Int. J. Pharm.* 400, 211 **(2010)**.

42. A. Cheng, H. Chan, K. F. To, W. K. Leung, K. K. Chan, C. T. Liew, and J. Sung, Cyclooxygenase-2 pathway correlates with vascular endothelial growth factor expression and tumor angiogenesis in hepatitis B virus-associated hepatocellular carcinoma. *Int. J. Oncol.* 24, 853 **(2004)**.

43. A. L. Cheng, C. H. Hsu, J. K. Lin, M. M. Hsu, Y. F. Ho, T. S. Shen, J. Y. Ko, J. T. Lin, B. R. Lin, and W. Ming-Shiang, Phase I clinical trial of curcumin, a chemopreventive agent, in patients with high-risk or pre-malignant lesions. *Anticancer. Res.* 21, 2895 **(2001)**.

44. C. D. Lao, M. T. Ruffin, D. Normolle, D. D. Heath, S. I. Murray, J. M. Bailey, M. E. Boggs, J. Crowell, C. L. Rock, and D. E. Brenner, Dose escalation of a curcuminoid formulation. BMC complement. *Altern. Med.* 6, 6 **(2006)**.

45. W. She, N. Li, K. Luo, C. Guo, G. Wang, Y. Geng, and Z. Gu, Dendronized heparin-doxorubicin conjugate based nanoparticle as pH-responsive drug delivery system for cancer therapy. *Biomaterials* 34, 2252 **(2013)**.

46. S.-D. Li and L. Huang, Pharmacokinetics and biodistribution of nanoparticles. *Mol. Pharm.* 5, 496 **(2008)**.